

# Pulse shaping by spectral-domain polarization gratings

ELVIS PILLINEN<sup>1</sup>, MATIAS KOIVUROVA<sup>2,3\*</sup>, AND JARI TURUNEN<sup>1</sup>

<sup>1</sup>Institute of Photonics, University of Eastern Finland, P.O. Box 111, FI-80101 Joensuu, Finland

<sup>2</sup>Tampere Institute for Advanced Study, Tampere University, 33100 Tampere, Finland

<sup>3</sup>Faculty of Engineering and Natural Sciences, Tampere University, 33720 Tampere, Finland

\*Corresponding author: matias.koivurova@tuni.fi

Compiled March 7, 2022

**We consider the spectral-domain counterparts of spatial-domain polarization gratings and study their effect on the temporal evolution of femtosecond-scale light pulses. These devices divide an incident light pulse to several orders via spectral polarization modulation, permitting pulse splitting and shaping with controlled time-domain polarization dynamics.** © 2022 Optica Publishing Group

<http://dx.doi.org/10.1364/ao.XX.XXXXXX>

Polarization gratings were introduced by Gori [1] as wire-grid-type polarizers whose polarization axis rotates linearly in the space domain (say, in the  $x$  direction), making a full circle within a period  $d$ . The periodicity of this particular polarization-modulating structure implies that the incident beam is split into (exactly) three diffracted orders, centered in the space-frequency domain at spatial frequencies dictated by the grating equation. If several periods  $d$  are illuminated by the incident beam, the diffraction orders become separated in the space-frequency domain. This enables, for instance, beam splitting and the measurement of the Stokes parameters of the incident beam [1]. On the other hand, if the illuminated region is of the order of  $d$  (or less), the three diffraction orders overlap. This facilitates, e.g., beam shaping and manipulation of the spatial coherence of incident partially spatially coherent fields [2]. We note that the operation of polarization gratings can also be interpreted by means of the Pancharatnam–Berry geometric phase [3].

Instead of spatially variable wire-grid polarizers, we may employ the phenomenon of form birefringence in dielectrics (Ref. [4], Sect. 15.5.2) to realize polarization gratings [5]. Such dielectric gratings with sub-wavelength local periodicity and a linearly rotating retardation axis enable more flexible control over the efficiencies of the three diffraction orders and their polarization states [5].

Here we introduce spectral-domain counterparts of space-domain polarization gratings. These devices are based on polarization modulation of the spectral field (as opposed to the spatial field). The three spectral-domain diffraction orders then create pulses that are either separated or overlap partially in the time domain (as opposed to space-frequency domain). The spectral-domain polarization gratings provide an addition to the reservoir of techniques for temporal pulse modulation of vectorial fields [6].

We assume that incident electromagnetic field consists of (a train of) fully coherent temporal plane-wave pulses with an envelop representation  $E_0(t) = A_0(t) \exp(-i\omega_0 t)$ , where  $\omega_0$  is the optical carrier frequency and  $A(t)$  is a column vector with elements  $A_{0x}(t)$  and  $A_{0y}(t)$  that specify the time-domain state of polarization of the field. The spectral field representation can then be expressed as

$$E_0(\tilde{\omega}) = \begin{bmatrix} E_{0x}(\tilde{\omega}) \\ E_{0y}(\tilde{\omega}) \end{bmatrix} = \frac{1}{2\pi} \int_{-\infty}^{\infty} A_0(t) \exp(i\tilde{\omega}t) dt, \quad (1)$$

where  $\tilde{\omega} = \omega - \omega_0$ . In the inverse relation

$$A_0(t) = \begin{bmatrix} A_{0x}(t) \\ A_{0y}(t) \end{bmatrix} = \int_0^{\infty} E_0(\omega) \exp(-i\tilde{\omega}t) d\tilde{\omega} \quad (2)$$

the lower integration limit (zero) can effectively be replaced by  $-\infty$  if the spectral width of the field is not too large or (by definition) contains no negative frequencies. From now on we take this to be the case.

Let the spectral field  $E_0(\tilde{\omega})$  be incident on a polarization modulating element SPG as illustrated in Fig. 1. The SPG can be described by a  $2 \times 2$  spectral transmission matrix

$$\mathbf{T}(\tilde{\omega}) = \begin{bmatrix} T_{xx}(\tilde{\omega}) & T_{xy}(\tilde{\omega}) \\ T_{yx}(\tilde{\omega}) & T_{yy}(\tilde{\omega}) \end{bmatrix}. \quad (3)$$

We assume that the matrix satisfies the periodicity condition  $\mathbf{T}(\tilde{\omega} + d) = \mathbf{T}(\tilde{\omega})$ , where  $d$  is the period of the spectral-domain grating, and expand it in a Fourier-series form

$$\mathbf{T}(\tilde{\omega}) = \sum_{m=-\infty}^{\infty} \mathbf{T}_m \exp(i2\pi m\tilde{\omega}/d), \quad (4)$$

where the coefficients  $\mathbf{T}_m$  are given by

$$\mathbf{T}_m = \frac{1}{d} \int_0^d \mathbf{T}(\tilde{\omega}) \exp(-i2\pi m\tilde{\omega}/d) d\tilde{\omega}. \quad (5)$$

The spectral field after the element is then  $E(\tilde{\omega}) = \mathbf{T}(\tilde{\omega})E_0(\tilde{\omega})$  and the temporal envelope of the output field becomes

$$A(t) = \sum_{m=-\infty}^{\infty} \mathbf{T}_m A_0(t - 2\pi m/d). \quad (6)$$

Hence the output field is a coherent superposition of temporally shifted terms corresponding to diffraction orders  $m$  of the spectral-domain grating. In general, each term has different polarization dynamics; only  $m = 0$  shares the polarization properties of the incident pulse.

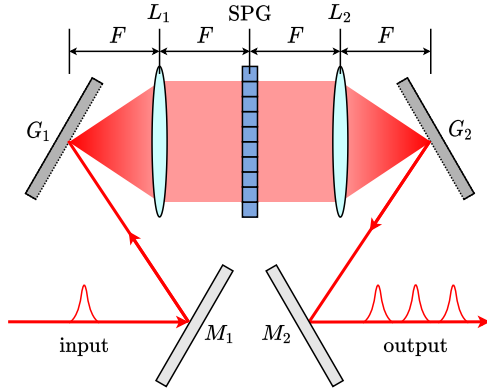


**Fig. 1.** Temporal pulse shaping by spectral polarization modulation. Here  $M_1$  and  $M_2$  are mirrors,  $G_1$  and  $G_2$  are gratings,  $L_1$  and  $L_2$  are achromatic lenses of focal length  $F$ , and SPG is a spectral polarization modulation device.

Let us now introduce spectral polarization gratings (SPGs) as spectral counterpart of the space-domain polarization grating by specifying the elements of  $\mathbf{T}(\tilde{\omega})$  as

$$T_{xx}(\tilde{\omega}) = A \cos^2(\pi\tilde{\omega}/d) + B \sin^2(\pi\tilde{\omega}/d), \quad (7a)$$

$$T_{xy}(\tilde{\omega}) = T_{yx}(\tilde{\omega}) = (A - B) \sin(\pi\tilde{\omega}/d) \cos(\pi\tilde{\omega}/d), \quad (7b)$$

$$T_{yy}(\tilde{\omega}) = A \sin^2(\pi\tilde{\omega}/d) + B \cos^2(\pi\tilde{\omega}/d), \quad (7c)$$

where  $A$  and  $B$  ( $A \leq 1$  and  $|B| \leq 1$ ) are the complex-amplitude spectral transmission coefficients for purely TE and TM polarized incident fields, respectively. The assumption that  $A$  and  $B$  are independent on frequency is not strictly true, but it is an excellent approximation especially with achromatic birefringent retarders [7, 8].

Inserting from Eqs. Eq. (7a)–(7c) into Eq. (5), we find that the coefficients  $\mathbf{T}_m$  are non-vanishing only for the three central diffraction orders  $m = -1, 0, +1$ , for which

$$\mathbf{T}_{-1} = \frac{1}{4}(A - B) \begin{bmatrix} 1 & i \\ i & -1 \end{bmatrix}, \quad (8a)$$

$$\mathbf{T}_0 = \frac{1}{2}(A + B) \begin{bmatrix} 1 & 0 \\ 0 & 1 \end{bmatrix}, \quad (8b)$$

$$\mathbf{T}_{+1} = \frac{1}{4}(A - B) \begin{bmatrix} 1 & -i \\ -i & -1 \end{bmatrix}. \quad (8c)$$

In general, we may then study the temporal properties using Eq. (6). For simplicity we assume that  $A_0(t) = A_0 f(t)$ , where  $A_0$  is a constant and  $f(t)$  is a scalar (square integrable) function. In other words, assume that the polarization state of the incident field is independent on time. Then the envelope of the output field takes the form

$$A(t) = A^{(-1)}(t) + A^{(0)}(t) + A^{(+1)}(t), \quad (9)$$

where

$$A^{(-1)}(t) = \frac{1}{4}(A - B) \begin{bmatrix} A_{0x} + iA_{0y} \\ iA_{0x} - A_{0y} \end{bmatrix} f(t + 2\pi/d), \quad (10a)$$

$$A^{(0)}(t) = \frac{1}{2}(A + B) \begin{bmatrix} A_{0x} \\ A_{0y} \end{bmatrix} f(t), \quad (10b)$$

$$A^{(+1)}(t) = \frac{1}{4}(A - B) \begin{bmatrix} A_{0x} - iA_{0y} \\ -iA_{0x} - A_{0y} \end{bmatrix} f(t - 2\pi/d). \quad (10c)$$

Clearly, if the effective temporal width of  $f(t)$  is sufficiently small in comparison with  $2\pi/d$ , the three sub-pulses separate and the polarization grating acts as a pulse splitter. This happens when the spectral field illuminates at least a few periods  $d$ . When the temporal width of  $f(t)$  is increased, the sub-pulses merge into a single temporally shaped pulse, which is the case if only a fraction of  $d$  is illuminated by the spectral field.

Generally, the polarization state of the output field is modulated temporally even if the incident field is not (as assumed before). The polarization dynamics of the output field can be conveniently described by time-domain Stokes parameters

$$S_0(t) = |A_x(t)|^2 + |A_y(t)|^2, \quad (11a)$$

$$S_1(t) = |A_x(t)|^2 - |A_y(t)|^2, \quad (11b)$$

$$S_2(t) = A_x^*(t)A_y(t) + A_y^*(t)A_x(t), \quad (11c)$$

$$S_3(t) = i [A_y^*(t)A_x(t) - A_x^*(t)A_y(t)]. \quad (11d)$$

The first parameter  $S_0(t)$  represents the intensity distribution, whereas the others characterize the temporal evolution of the polarization state of the output pulses. These parameters are closely related to the temporal evolution of the polarization axis and ellipticity of the time-dependent polarization ellipse, in analogy with the monochromatic case described in Ref. [4], Sect. 1.4.2(c).

To illustrate the effects described qualitatively above, we take the temporal wave form of the incident pulse envelope as a Gaussian function  $f(t) = \exp(-t^2/T^2)$ , where  $T$  is a measure of pulse duration. The spectral field is then  $E_0(\tilde{\omega}) = E_0 \exp(-\tilde{\omega}^2/\Omega^2)$ , where  $E_0 = A_0/\sqrt{\pi}\Omega$  and  $\Omega = 2/T$  is the characteristic spectral width of the pulses. Several grating periods are illuminated in the spectral domain when  $\Omega \gg d$  and hence the temporal pulses are well separated if  $T \ll 2\pi/d$ .

The choice of the parameters  $A$  and  $B$ , as well as the state of polarization of the incident field, affect the mutual weights and the polarization states of the three components in Eq. (9) in analogy with the spatial case [5]. The polarization grating is lossless if  $|A| = |B| = 1$ . In the following, we consider three particular examples in analogy with Ref. [5] and plot the intensity  $S_0(t)$  as well as the normalized Stokes parameters, defined as  $s_j(t) = S_j(t)/S_0$ ,  $j = 0, 1, 2, 3$ . We use a normalized time coordinate  $t/(2\pi/d)$  to place the centers of the orders at integer positions on the time axis. In all figures the black line shows  $S_0(t)$ . In all cases  $s_1(t) = 0$ ; the red and blue lines refer to  $s_2(t)$  and  $s_3(t)$ , respectively.

In the first example (Fig. 2) we take a 45° linearly polarized input field with  $A_{0x} = A_{0y} = 1/\sqrt{2}$ , and a half-wave SPG with  $A = 1$  and  $B = -1$ . With these choices the  $m = 0$  (zeroth-order) term vanishes, resulting in a lossless temporal pulse duplicator. The  $m = -1$  sub-pulse is left-hand circularly polarized (LCP)

while the  $m = +1$  sub-pulse is right-hand circularly polarized (RCP). When the subpulses begin to overlap, as in Fig. 2(a), there is a region of growing width, where a smooth transition from LCP to RCP takes place and also the ellipticity varies, as seen from  $s_3(t)$ . When the overlap is chosen suitably, such as in Fig. 2(c), we obtain a pulse with a flat region in the center. In this case (and for larger values of  $T$ ), the variation of rotation axis as well as the ellipticity extend effectively over the entire temporal width of the pulse.

In the second example (Fig. 3) we employ an LCP input beam with  $A_{0x} = 1/\sqrt{2}$ ,  $A_{0y} = i/\sqrt{2}$ , and a quarter-wave SPG with  $A = 1$  and  $B = \exp(-i\pi/2)$ . With these choices the  $m = -1$  term vanishes, resulting in a lossless temporal pulse duplicator with orders  $m = 0$  and  $m = 1$ . When the sub-pulses are temporally separate, the  $m = 0$  sub-pulse has (as always) the same polarization state as the incident pulse (in this case LCP) while the  $m = 1$  sub-pulse is RCP. When the temporal overlap begins, there is again a region in between the pulses where the transition becomes gradual. As with the previous example, the incident pulse can be shaped in a flat-topped pulse of increased temporal width. Moreover, if we instead assume that the incident pulse is RCP, we have orders  $m = -1$  and  $m = 0$ , and corresponding conclusion can be drawn.

In the third example (Fig. 4) we assume a TE polarized linearly polarized input field with  $A_{0x} = 1$  and  $A_{0y} = 0$ , and consider an SPG with  $A = 1$  and  $B = \exp(i\varphi)$  with  $\cos \varphi = -1/3$ . We now get a temporal pulse triplicator. The  $m = -1$  sub-pulse is LCP, the  $m = 0$  sub-pulse is TE polarized, and the  $m = +1$  sub-pulse is RCP. When the overlap begins, smooth transitions from LCP to linear polarization and from linear to RCP polarization appear as shown in Fig. 4(a). A further increase of  $T$  leads to a flat-top pulse. As seen from Fig. 4(b), the flat region is now wider than in the previous examples since three orders are employed to generate it.

We note that polarization gratings with more than three diffraction orders can be designed [9], which also have direct spectral-domain analogues. When the diffraction orders are separated in time, we then have  $1 \rightarrow N$  splitters with exactly  $N$  signal pulses and no undesired sub-pulses. However, merging the signal pulses by increasing  $T$  does not in general lead to flat-top pulses because of the specific phase relations of different orders required to equalize the efficiencies. The role of these phase relations is already evident for the triplicator: flat-top generation works for purely TE (or TM) incident fields, but for arbitrarily linearly polarized incident pulses the interference between the overlapping orders causes irregular pulse shapes.

We have introduced polarization gratings operating in the spectral rather than the spatial domain and studied the ensuing temporal effects, assuming that SPGs are realized using form-birefringence of subwavelength-period surface-relief gratings with a linearly rotating retardation axis. These can be manufactured with lithographic techniques [10]. Considering the limitations of this technique, two issues arise. The first is the spectral variation of the retardation. However, since the bandwidths of 100-fs-scale pulses are in 10 nm range in the wavelength scale, the variations are rather negligible. The second issue is that, in practice, the linear variation of the orientation angle  $\theta$  must be discretized to  $Q$  steps (with a constant value of  $\theta$  in each) per grating period  $d$ . This reduces the conversion efficiency slightly, as discussed in Ref. [9], to  $\eta = \sin^2(\pi Q)/(\pi Q)^2$ . However, in our case  $d$  is on the order of the spectral bandwidth of the incident pulses, which would in a practical realizations of the setup

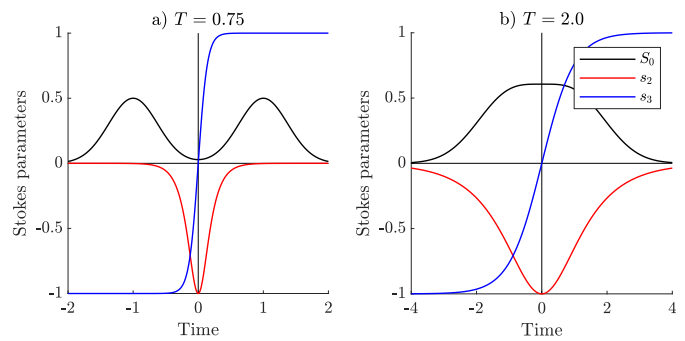


**Fig. 2.** Example 1: Temporal Stokes parameters  $S_0(t)$ ,  $s_2(t)$ , and  $s_3(t)$  as functions of normalized time  $t/(2\pi/d)$  for a duplicator with diffraction orders  $m = \pm 1$ . (a)  $T = 0.75$ . (b)  $T = 2.0$ . Black:  $S_0(t)$ . Red:  $s_2(t)$ . Blue:  $s_3(t)$ .

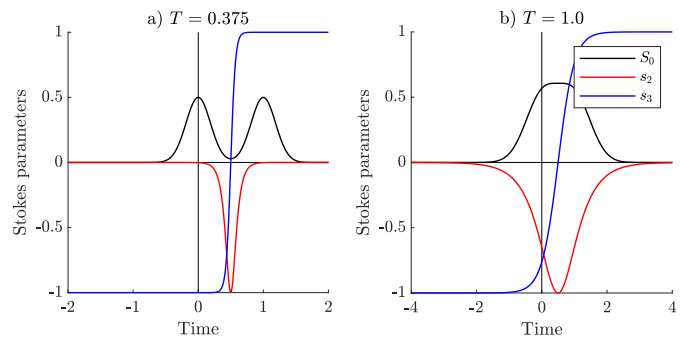


**Fig. 3.** Example 2: Same as Fig. 2 but for a duplicator with orders  $m = 0$  and  $m = 1$ . (a)  $T = 0.375$ . (b)  $T = 1.0$ .

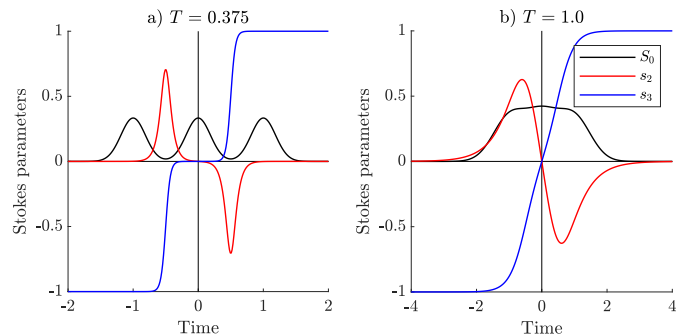


**Fig. 4.** Example 4: Same as Fig. 2 but for a triplicator with orders  $m = 0$  and  $m = \pm 1$ . (a)  $T = 0.375$ . (b)  $T = 1.0$ .

of Fig. 1 be in the millimeter range. Hence, when the grating is manufactured using the techniques of Ref. [7, 8],  $Q$  can be made sufficiently large to ensure that  $\eta \rightarrow 1$ .

Experimental characterization of the polarization properties can be accomplished using standard polarization components at the output of the system in Fig. 1 in a set of configurations that allow the determination of the Stokes parameters for stationary light [11]. The measurement of the time-dependent Stokes parameters  $S_j(t)$  is then possible by any well-established pulse characterization technique [12], such as Frequency-Resolved Optical Gating (FROG).

We have assumed throughout this paper that the incident pulse train is fully coherent, i.e., strictly periodic with each individual pulse having the same (Gaussian) temporal profile.

This assumption is well-justified for femtosecond pulse trains produced by mode-locked lasers operating in stable conditions. In the presence of noise, there may be some randomness in the arrival times of the incident pulses (pulse jitter). However, this will not show up in FROG measurements because of the inherent arrival-time ambiguity in such measurements. Another effect of noise, which FROG would see, is a pulse-to-pulse shape variation. This makes the output pulse train spectrally and temporally partially coherent [12]. To obtain the average properties of the pulse train, one would then measure an ensemble of individual output pulses and subsequently construct the two-frequency cross-spectral density function and the two-time mutual coherence function by taking ensemble averages over the individual-pulse realizations.

The optical functionality of the SPGs can be achieved by any technique that provides independent control of the  $x$  and  $y$  components of the spectral field [6]. In particular, techniques based on spatial light modulators permit real-time control of the parameters that define the SPG. In fact, the effect of SPGs on the intensity distribution of output pulses has recently been studied experimentally with liquid-crystal devices [13].

We envisage the SPGs discussed here to be useful in numerous applications that require temporal pulse shaping [6]. In particular, it is worth noting that a birefringent crystal in the time domain has been recently used to produce spectrally varying polarization rotation [14], which essentially constitutes an inverse of SPG operation.

## ACKNOWLEDGMENTS

This research was funded by the Academy of Finland (project 333938). It is part of the Academy of Finland's flagship program 'Photonics Research and Innovation' (PREIN, 320165, 320166).

## DISCLOSURES

The authors declare no conflicts of interest.

## REFERENCES

1. F. Gori, *Opt. Lett.* **24**, 584–586 (1999).
2. G. Piquero, R. Borghi, and M. Santarsiero, *J. Opt. Soc. Am. A* **18**, 1399–1405 (2001).
3. Z. Bomzon, G. Biener, V. Kleiner, and E. Hasman, *Opt. Lett.* **25**, 1141–1143 (2000).
4. M. Born and E. Wolf, *Principles of Optics* (Cambridge, 2013).
5. J. Tervo and J. Turunen, *Opt. Lett.* **25**, 785–786 (2000).
6. K. Misawa, *Adv. Phys.: X* **1**:4, 544–569 (2016).
7. H. Kikuta, Y. Ohira, and K. Iwata, *Appl. Opt.* **36**, 1566–1572 (1997).
8. G. P. Nordin and P. C. Deguzman, *Opt. Express* **5**, 163–168 (1999).
9. M. Honkanen, V. Kettunen, J. Tervo, and J. Turunen, *J. Mod. Opt.* **47**, 2351–2359 (2000).
10. I. Vartiainen, J. Tervo, J. Turunen, and M. Kuittinen, *Opt. Express* **18**, 22850 (2010).
11. L. Mandel and E. Wolf, *Coherence and Quantum Optics* (Cambridge University Press, 1995), Sec. 6.2.
12. I. A. Walmsley and C. Dorrer, *Adv. Opt. Photon.* **1**, 308–437 (2009).
13. B. Gökce, Y. Li, M. J. Escuti, and K. Gundogdu, *Opt. Lett.* **39**, 1521–1524 (2014).
14. L. Kopf, J. R. D. Ruano, M. Hiekkamäki, T. Stolt, M. J. Huttunen, F. Bouchard, and R. Fickler, *Optica* **8**, 930–935 (2021).

## REFERENCES

1. F. Gori, "Measuring Stokes parameters by means of a polarization grating," *Opt. Lett.* **24**, 584–586 (1999).
2. G. Piquero, R. Borghi, and M. Santarsiero, "Gaussian Schell-model beams propagating through polarization gratings," *J. Opt. Soc. Am. A* **18**, 1399–1405 (2001).
3. Z. Bomzon, G. Biener, V. Kleiner, and E. Hasman, "Space-variant Pancharatnam–Berry phase optical elements with computer-generated subwavelength gratings," *Opt. Lett.* **25**, 1141–1143 (2000).
4. M. Born and E. Wolf, *Principles of Optics* (Cambridge, 2013).
5. J. Tervo and J. Turunen, "Paraxial-domain diffractive elements with 100% efficiency based on polarization gratings," *Opt. Lett.* **25**, 785–786 (2000).
6. K. Misawa, "Applications of polarization-shaped femtosecond laser pulses," *Adv. Phys.: X* **1**:4, 544–569 (2016).
7. H. Kikuta, Y. Ohira, and K. Iwata, "Achromatic quarter-wave plates using the dispersion of form birefringence," *Appl. Opt.* **36**, 1566–1572 (1997).
8. G. P. Nordin and P. C. Deguzman, "Broadband form birefringent quarter-wave plate for the mid-infrared wavelength region," *Opt. Express* **5**, 163–168 (1999).
9. M. Honkanen, V. Kettunen, J. Tervo, and J. Turunen, "Fourier array illuminators with 100% efficiency: analytical Jones-matrix construction," *J. Mod. Opt.* **47**, 2351–2359 (2000).
10. I. Vartiainen, J. Tervo, J. Turunen, and M. Kuittinen, "Surface-relief polarization gratings for visible light," *Opt. Express* **18**, 22850 (2010).
11. L. Mandel and E. Wolf, *Coherence and Quantum Optics* (Cambridge University Press, 1995), Sec. 6.2.
12. I. A. Walmsley and C. Dorrer, "Characterization of ultrashort electromagnetic pulses," *Adv. Opt. Photon.* **1**, 308–437 (2009).
13. B. Gökce, Y. Li, M. J. Escuti, and K. Gundogdu, "Femtosecond pulse shaping using the geometric phase," *Opt. Lett.* **39**, 1521–1524 (2014).
14. L. Kopf, J. R. D. Ruano, M. Hiekkamäki, T. Stolt, M. J. Huttunen, F. Bouchard, and R. Fickler, "Spectral vector beams for high-speed spectroscopic measurements," *Optica* **8**, 930–935 (2021).